AIAA 96-1867

Comparison of Experimental and Computational Aerothermodynamics of a 70-deg Sphere-Cone

Brian R. Hollis and John N. Perkins
North Carolina State University
Raleigh, NC

31st AIAA Thermophysics Conference

June 18-20, 1996 / New Orleans, LA

Comparison of Experimental and Computational Aerothermodynamics of a 70-deg Sphere-Cone

Brian R. Hollis* and John N. Perkins†
Department of Mechanical and Aerospace Engineering
North Carolina State University
Raleigh, NC 27695-7910

ABSTRACT

Numerical solutions for hypersonic flows of carbon-dioxide and air around a 70-deg sphere-cone have been computed using an axisymmetric non-equilibrium Navier-Stokes solver. Freestream flow conditions for these computations were equivalent to those obtained in an experimental blunt-body heat-transfer study conducted in a high-enthalpy, hypervelocity expansion tube. Comparisons have been made between the computed and measured surface heat-transfer rates on the forebody and afterbody of the sphere-cone and on the sting which supported the test model. Computed forebody heating rates were within the estimated experimental uncertainties of ±10% on the forebody and ±15% in the wake except for within the recirculating flow region of the wake.

NOMENCLATURE

h	enthalpy (J/kg)
Kn	Knudsen number
M	Mach number
p	pressure (N/m^2)
q	heat transfer rate (W/m^2)
R_b	forebody radius (m)
Re	Reynolds number
S	distance along model surface (m)
T	temperature (K)
Δt_{est}	flow establishment time (sec)
U_∞	freestream velocity (m/sec)
Y_s	species mass fraction
y_{ref}	reference length (m)
ρ	density (kg/m^3)
σ	standard deviation
τ	establishment parameter, $\tau = U_4 \Delta t_{est} / y_{ref}$

Subscripts:

0	total
1	freestream
2	post normal shock

INTRODUCTION

In recent years, NASA has embarked on a long-term exploration initiative[1] in which unmanned orbiters and landers will be employed to gather scientific data on the planet Mars. This initiative has produced renewed interest in blunt-body entry vehicle and aerobrake configurations such as the 70-deg sphere-cone geometry of the Mars-Pathfinder (formerly known as MESUR) spacecraft[2]. This interest has led to a number of computational and experimental studies of blunt-body flows in perfect-gas[3,4], high-enthalpy[4-8], and rarefied[9-11] environments.

The present work contributes to the growing data base on blunt-body flows through the presentation of comparisons between surface heat-transfer rates measured in a high-enthalpy test facility and heat-transfer rates obtained from flow field solutions computed using a nonequilibrium Navier-Stokes solver. These comparisons were made for test environments (CO_2 and N_2-O_2) representative of the atmospheres of

---

* Graduate Researcher, AIAA Member

† Professor, Mechanical and Aerospace Engineering Dept., Associate Fellow AIAA

Mars and Earth, and encompassed both the forebody and wake (that is, the afterbody and model sting) regions of the flow.

The subject of these comparisons was a 70-deg sphere-cone configuration (Fig. 1) derived from the geometry of the Mars-Pathfinder spacecraft. The radius of the sphere-cone forebody was 2.54 cm (1 inch). The forebody had a nose-to-forebody-radius ratio of 0.5 and a corner-to-forebody-radius ratio of 0.05. This configuration also had a 40-deg cone-frustrum afterbody which represented the payload section of the vehicle. The cone-frustrum angle was altered from that of Mars-Pathfinder (49.5 deg) in order to accommodate the sting which was used to support the model in the test facility. This sting was fully instrumented with heat-transfer gages and was included in the geometry definition for the numerical computations. The location of reference points on the model in terms of normalized surface distance, S/R_b, from the forebody stagnation point are given in Fig. 2.

Although this research encompassed both the forebody and wake regions of the sphere-cone configuration, emphasis was placed on measurements and computations for the wake of the configuration. The important features of a blunt-body wake flow field (Fig. 3) are: a free shear layer formed by the separation of the forebody boundary layer at or around the corner of the vehicle; a large recirculating flow region bordering on the afterbody and base of the vehicle; a shear-layer impingement point on the sting (or a "neck" region in the case of actual spacecraft, which would not have a sting); and a recompression shock formed as the shear layer is turned back into the direction of the freestream. These features define the aerothermodynamic environment of the wake, and their behavior influences the design of an aerobrake or entry vehicle. Thermal protection shielding on the payload of the vehicle must be sufficient to withstand the aerothermodynamic loads imposed upon it, and the size and placement of the payload must be such that the wake free-shear layer does not impinge upon it or a localized region of high heating will be produced.

EXPERIMENT DESCRIPTION

Heat-transfer test models of the 70-deg sphere-cone geometry were fabricated from Macor (a trademark name of Corning, Inc.), a thermally-insulative, machineable glass-ceramic material, and were instrumented with fast-response thin-film heat-transfer gages[12]. Model stings were fabricated from stainless steel and included a slot into which a contoured Macor insert with additional gages was fitted. Each model and sting combination had a total of 70 thin-film gages (Fig. 4) which provided instrumentation coverage on the forebody and afterbody of the model and on the sting.

These models were tested in the NASA HYPULSE Expansion Tube[13], which is operated by the General Applied Sciences Laboratories (GASL). The HYPULSE Expansion Tube is an impulse facility in which high-enthalpy, hypervelocity flows can be produced using a variety of test gases. The HYPULSE facility is used in the study of high-temperature, chemically-reacting flow fields such as those inside a scramjet[14] or around a planetary entry vehicle[15]. The details of the present HYPULSE blunt-body heating study are presented in full in Refs. 4 and 6.

Freestream flow properties for the air and CO_2 test conditions at which HYPULSE was operated during this study are presented in Table 1. Nondimensional simulation parameters for these test conditions are listed in Table 2. The flow properties were computed using the ERGAS[16] (Equilibrium Reacting Gas) code with measured static pressures, shock speeds and pitot pressure calibration data as inputs. Uncertainty estimates in Table 1 for the flow properties are defined by two standard deviations (σ) of the mean values computed from the data from 26 CO_2 and 20 air runs conducted during this research.

The values from Table 1 were used to define the freestream boundary conditions for the numerical solution of the Navier-Stokes equations. Of these properties, the freestream density and velocity are the factors which have the greatest influence or aerodynamic heating[17]:

$$q \propto \rho_1^{0.5} U_1^3 \tag{1}$$

As the uncertainty in these properties was estimated to be no more than ±1% for velocity and no more than ±3% for density, it can be expected that the uncertainty introduced into numerical computations by the freestream properties specification will be small.

During the HYPULSE tests, gage data were sampled at 500 kHz over a test window of ~150 μsec. Gage data in the form of voltage time-histories were

converted to temperature time-histories using pre-test voltage-temperature calibrations. The temperature time-histories were then used as inputs to the 1DHEAT[18] data reduction code. This code was used to compute surface heat-transfer rates through both a closed-form analytical method[19] and a finite-volume solution for the temperature distribution within the model. In both methods, one-dimensional heat conduction into the model is assumed. The analytical method includes an empirical correction for the variation of the thermal properties of Macor with temperature, while the temperature dependence of Macor properties is incorporated into the formulation of the finite-volume method.

Owing to the short duration of HYPULSE tests, the model surface temperature increase was no more than 150 K at the forebody stagnation point and was considerably less elsewhere on the model. This increase was negligible in relation to the flow field total temperatures (6026 K in air and 3703 K in CO_2), which drive the surface heat-transfer rates. Therefore, surface heat-transfer rates essentially remained constant except for the effects of experimental noise and the wake flow establishment process. Experimental results reported thus are taken to be at a uniform ambient wall temperature of 300 K.

In order to eliminate the effects of experimental noise, surface heat-transfer rates were averaged over the data acquisition window of each test. Experimental uncertainty was estimated by two standard deviations from the mean values determined for each test. Forebody heat-transfer rate uncertainty was estimated to be no more than ±10%. Owing to the much lower (one to two orders of magnitude) heating in the wake, signal-to-noise ratios were higher, and thus a greater uncertainty level of ±15% was computed.

The wake flow establishment process was thoroughly investigated[4] in order to insure the validity of the data reported for use in comparisons to computational results. This was necessary because the time required for the flow in the wake of a blunt-body to become fully established can represent a significant fraction of the total available test time. Transient data obtained during this establishment process cannot be included in the data-averaging process or the resulting mean values will be inaccurate. It was found that flow establishment in HYPULSE required ~60 flow-path lengths in CO_2 tests and ~70 flow-path lengths in air tests. Flow-path lengths are defined by the non-dimensional establishment parameter, τ:

$$\tau = \frac{U_4 \Delta t}{y_{ref}} \tag{2}$$

where y_{ref} is the difference between the forebody and sting radii. The values computed for establishment in air and CO_2 represent approximately 75% of the duration of a HYPULSE test and are consistent with past research[20].

Several runs were made at each of the HYPULSE test points. The experimental data from theses runs are presented in Figs. 5 and 6. Average values based on the data from all of the runs for each test condition are also shown in these figures.

CODE DESCRIPTION

Numerical solutions of the Navier-Stokes equations for hypersonic flows[21] were computed using the NEQ2D[22] code. NEQ2D is an implicit, two-dimensional/axisymmetric Navier-Stokes solver. Solution of the governing equation set is accomplished in NEQ2D through the use of the line Gauss-Seidel technique[23]. Inviscid fluxes are computed through a modified Steger-Warming[23] flux-splitting technique, which minimizes numerical dissipation in boundary layers. In high pressure gradient regions, such as near the bow shock, the flux-splitting method reverts to the original Steger-Warming technique in order to maintain numerical stability. Viscous fluxes are computed through second-order central differences. Vibrational nonequilibrium is represented through the two-temperature model of Park[24]. Non-ionizing thermochemical models in NEQ2D for Earth (N_2-O_2-NO-N-O) and Mars[25] (CO_2-CO-N_2-O_2-NO-C-N-O) atmospheres were employed in this study.

Freestream boundary conditions for the air and CO_2 cases were taken from Table 1. Freestream species mass fractions were Y_{CO2} = 1.00 for the CO_2 case and Y_{N2} = 0.76533 and Y_{O2} = 0.23467 for the air case. Wall temperatures were set to a uniform value of 300 K. Owing to the low surface temperature, a non-catalytic wall boundary condition was specified.

GRID GENERATION, ADAPTATION AND REFINEMENT

Initial grids of 125 x 90 points in the streamwise and normal directions for the two test cases were constructed using an elliptical grid generation code. The grids were separated into forebody and wake zones along the normal grid line from the outermost point on the forebody corner. Flow field distributions at the supersonic outflow boundaries of the forebody grids were used as starting conditions for solutions on the wake grids.

A grid adaptation scheme based on the algorithm described by Gnoffo[26] was employed to align the streamwise grid lines with the bow shock and to cluster points in the wall boundary layer. The height of the first cell at the wall initially was set to a cell Reynolds number (based on local sonic speed) of $O(1)$. However, it was found that the extremely large differences in density between the forebody and wake flows resulted in unreasonably large cell growth in the separated flow region of the wake when all wall cells were fixed at a uniform Reynolds number. Instead, cell heights were set to a uniform value for all wall cells. Test computations were performed with wall cell heights of between $1x10^{-7}$ m and $1x10^{-5}$ m; it was found that the wall heating results were nearly invariant for cell heights ($\sim 1x10^{-6}$ m) which produced cell Reynolds numbers of $O(10)$ or below.

After solutions were computed on the original grids for the CO_2 and air cases (these are the results presented in Ref 6.), shear-layer adapted grids were created through the use of the VGM (Volume Grid Manipulator) code. VGM was employed to cluster streamwise grid lines in the region of the wake free shear layer and within the wake recirculation zone. The adapted grids for the two test cases are shown in Figs. 7a-b and 8a-b. This grid adaptation had a significant effect on surface heat transfer rates on the afterbody and sting, as will be discussed in the next section. Grids of 125 x 45 and 125 x 180 points also were constructed from the adapted 125 x 90 point grids in order to investigate the effects of grid refinement on the computational solutions.

COMPUTATIONAL RESULTS AND COMPARISON WITH EXPERIMENT

Non-dimensionalized heat-transfer and surface pressure distributions for the CO_2 and air cases (from the fine 125 x 180 point grids) are presented in Figs. 9a and 9b for the forebody and for the afterbody and sting, respectively. The effects of grid adaptation and refinement on the surface heat-transfer distributions for the CO_2 and air cases are shown in Figs 10a–b and 11a–b, respectively.

The CO_2 case forebody pressure distribution (Fig. 9a) showed an over-expansion and recompression at the sphere-cone junction, while the influence of the corner extended slightly further upstream for the air case. These effects were reflected in the shape of the non-dimensional heating distributions in these areas. Wake heating distributions were one to two orders of magnitude lower than on the forebody for both test cases (Fig. 9b). Local heating maxima were produced on the afterbody where the flow was accelerated around the corner at $S/R_b = 1.72$, and where the wake free shear layer impinged on the sting ($S/R_b = 3.5$ for CO_2 and $S/R_b = 4$ for air).

For both CO_2 and air cases, a significant decrease in heating (~10%) on the forebody was observed between the coarse 125 x 45 grids and the intermediate 125 x 90 point grids (Figs. 10a and 11a). Forebody heating rates decreased by no more than 2% between the intermediate grids and the fine 125 x 180 point grids. Shear layer adaption affected only the wake portion of the grids, and so there were no changes in the heating rates computed on the original and adapted 125 x 90 point grids.

As was observed in other studies[8], the surface heating rates on the afterbody and sting proved to be sensitive to both the resolution and point-distribution of the grids. This was due to the existence of a large region of separated, recirculating flow behind the model. As shown in Figs. 12 and 13., this vortex extended approximately 1-1/2 body radii downstream from the base of the model for both test cases. Smaller, counter-rotating vortices also were produced where the flow in the main vortex was turned at the model/sting junction and at the corner on the afterbody.

It was because of the viscous nature of the shear layer and the complicated recirculating flow patterns that the original 125 x 90 point grids were adapted to provide better resolution within this region. As shown in Figs. 10b and 11b, grid adaption had two effects: first, the magnitude of the surface heating rates within the recirculation region decreased (the value of the local heating peak on the sting was reduced by

~30% for the CO_2 case and ~10% for the air cases); second, the heating peak was moved approximately half a body radius further away from the model. The same effects, although of smaller magnitude, were observed when the number of normal points in the adapted grids was increased from 45 to 90 points and from 90 to 180 points. It also was noted that the heating distributions downstream of the wake vortex were affected only minimally by either grid adaptation of refinement.

Heating distributions computed on the fine 125 x 180 point grids are compared to the averaged values from the experimental data on Figs. 14 and 15. Note that the forebody and wake heating distributions are plotted on separate linear y-axes in order to resolve the details in both regions. Error bars on the experimental data represent the uncertainty estimates of ±10% for the forebody and ±15% for the wake. Computed forebody heating rates were within the uncertainty bands of the experimental data. The computed wake heating rates for the air case were approximately 25% lower than the experimental data within the recirculation zone, but approached the experimental data downstream from the shear layer impingement point. For the CO_2 case, computed wake heating rates were approximately 25% higher than the experimental data in the center of the recirculation region, but were within the experimental uncertainty band around the impingement point and further downstream on the sting.

It is worth noting that the effects of grid adaptation and grid resolution were favorable in terms of comparisons with the experimental data. Adaptation and refinement moved the peak heating point further downstream, which brought it into good agreement with the experimentally determined location. This also lowered the heating rates in the recirculation zone, which made the comparison with experiment in this region more favorable. As agreement between the two sets of data is already good outside of the recirculation zone, further adaptation of the grid point distribution within this region would probably be more computationally efficient than a global increase in the number of grids points. This course of action is currently being pursued.

SUMMARY AND CONCLUSIONS

Numerical solutions for the forebody and wake flow around a 70-deg sphere-cone in CO_2 and air were computed using a non-equilibrium Navier-Stokes solver. Freestream conditions for these computations were equivalent to those at which tests were conducted in a high-enthalpy, hypervelocity expansion tube. Comparisons were made between these results of these computations and the experimental data. The experimental and computational forebody results were found to agree to within less than the estimated experimental uncertainty of ±10% for this region. The sensitivity of wake computations to grid resolution and to the distribution of grid points within the wake free shear layer and recirculation region was demonstrated. Computed wake results for the air test case fell outside of the estimated experimental uncertainty of ±15% for the wake, although the discrepancies appeared to decrease with distance from the recirculation zone. With the exception of a small region in the center of the recirculation zone, computed wake results for the CO_2 case were within the estimated range of experimental uncertainty.

ACKNOWLEDGMENTS

This research was conducted under NASA grants NAGW-1331 and NAG1-1663 to North Carolina State University. Computer time on the NASA Langley Research Center Cray Y-MP and funding for model fabrication and testing in HYPULSE was provided by the Aerothermodynamics Branch of NASA Langley. The authors wish to thank: Graham Candler of the University of Minnesota for the use of the NEQ2D code; Stephen Alter of Lockheed-Martin for the use of the VGM code; and John Calleja of GASL for assistance in the tests conducted in the HYPULSE facility.

REFERENCES

(1) Bourke, R.D., Golombek, M. P., Spear, A. J., and Sturms, F. M., "MESUR and Its Role in an Evolutionary Mars Exploration Program," IAF Paper 92-0509, 1992.

(2) Wercinski, P. F., "Mars Aerocapture Analysis for the MESUR/Mars-Pathfinder Aeroshell in Low L/D Configurations," AIAA Paper 95-3495.

(3) Horvath, T. J., McGinley, C. B., and Hannemann, K., "Blunt Body Near Wake Flow Field at Mach 6," AIAA Paper 96-1935, June 1996.

(4) Hollis, B. R., and Perkins, J. N., "High-Enthalpy and Perfect-Gas Heating Measurements on a Blunt Cone," Accepted for publication in *AIAA Journal of Spacecraft and Rockets*, 1996.

(5) Kastell, D., Horvath, T. J., and Eitelberg, G., "Nonequilibrium Flow Expansion Around a Blunted Cone," 2nd European Symposium on Aerothermodynamics, ESTEC, Noordwijk, The Netherlands, Nov., 1994.

(6) Hollis, B. R., Perkins, J. N., "Hypervelocity Heat-Transfer Measurements in an Expansion Tube," AIAA Paper 96-2240, June 1996.

(7) Mitchletree, R. A., and Gnoffo, P. A., "Wake Flow About a MESUR Mars Entry Vehicle," AIAA Paper 94-1958, June 1994.

(8) Haas, B. L., and Venkatapathy, E., "Mars Pathfinder Computations Including Base-Heating Predictions," AIAA Paper 95-2086, June 1995.

(9) Allegre, J., and Bisch, D., "Blunted Cone at Rarefied Hypersonic Conditions. Experimental Density Flow Fields, Heating Rates and Aerodynamic Forces," CNRS Report RC 95-2, Sept. 1995.

(10) Holden, M., Kolly, J., and Chadwick, K. "Calibration, Validation and Evaluation Studies in the LENS Facility," AIAA Paper 95-0291, Jan. 1995.

(11) Moss, J. N., Price, J. M., Dogra, V. K., and Hash, D. B., "Comparison of DSMC and Experimental Results for Hypersonic External Flows," AIAA Paper 95-2028, June 1995.

(12) Miller, C. G., "Comparison of Thin-Film Resistance Heat-Transfer Gages with Thin-Skin Transient Calorimeter Gages in Conventional Hypersonic Wind Tunnels," NASA TM 83197, Dec., 1981.

(13) Tamagno, J., Bakos, R., Pulsonetti, M., and Erdos, J., "Hypervelocity Real Gas Capabilities of GASL's Expansion Tube (HYPULSE) Facility," AIAA Paper 90-1390, June 1990.

(14) Bakos, R., Tamagno, J., Rizkalla, O., Pulsonetti, M., and Chinitz, W., "Hypersonic Mixing and Combustion Studies in the GASL HYPULSE Facility," AIAA Paper 90-2095, June 1990.

(15) Calleja, J., Trucco, R., Tamagno, J., and Erdos, J., "Results of Hypervelocity Aeroheating Tests of Aeroassist Flight Experiment (AFE) Forebody Models in Air, Helium, and CO_2," GASL TR 326, Oct. 1990.

(16) Miller, C. G., "Computer Program of Data Reduction Procedures for Facilities using CO_2-N_2-O_2-Ar Equilibrium Real-Gas Mixtures," NASA TMX–2512, March, 1972.

(17) Anderson, J. D., Hypersonic and High Temperature Gas Dynamics, McGraw-Hill, Inc., 1989.

(18) Hollis, B. R., "User's Manual for the One–Dimensional Hypersonic Aero-Thermodynamic (1DHEAT) Data Reduction Code," NASA CR 4691, August, 1995.

(19) Kendall, D. N., Dixon, W. P., and Schulte, E. H., "Semiconductor Surface Thermocouples for Determining Heat-Transfer Rates," *IEEE Transactions on Aerospace and Electronic Systems*, Vol. AES-3, No. 4, July 1967, pp. 596-603.

(20) Holden, M. S., "Development and Code Evaluation Studies in Hypervelocity Flows in the LENS Facility," 2nd European Symposium on Aerothermodynamics for Space Vehicles, ESTEC, Noordwijk, The Netherlands, Nov., 1994.

(21) Lee, J. H., "Basic Governing Equations for the Flight Regimes of Aeroassisted Orbital Transfer Vehicles," *Thermal Design of Aeroassisted Orbital Transfer Vehicles*, ed. H. F. Nelson, Progress in Aeronautics and Astronautics, Vol. 96, pp. 3-53, 1985.

(22) Candler, G. V., and MacCormack, R. W., "Computation of Weakly Ionized Flows in Thermochemical Nonequilibrium," *AIAA Journal of Thermophysics and Heat Transfer*,

Vol. 5, No. 3, pp. 226-273, 1991.

(23) Candler, G. V., and MacCormack, R. W., "The Solution of the Navier-Stokes Equations Using Gauss-Seidel Line Relaxation," *Computers and Fluids*, Vol. 17, No. 1, pp. 135-150, 1989.

(24) Park, C., "Assessment of the Two-Temperature Kinetic Model for Ionizing Air," AIAA Paper 87-1574, 1987.

(25) Candler, G. V., "Computation of Thermo-Chemical Nonequilibrium Martian Atmospheric Entry Flows." AIAA Paper 90-1695, June 1990.

(26) Gnoffo, P. A., Hartung, L. C., and Greendyke, R. B., "Heating Analysis for a Lunar Transfer Vehicle at Near-Equilibrium Conditions," AIAA Paper 93-0270, Jan. 1993.

Table 1. HYPULSE Test Conditions

Test Gas	p_1 (g/m^3)	U_1 (m/s)	T_1 (K)	P_1 (Pa)	$h_0 - h_{298K}$ (MJ/kg)	$P_{0,2}$ (MPa)	$T_{0,2}$ (K)
CO_2	5.789±3.1%	4772±1.1%	1088±8.7%	1187±10.8%	12.25±2.1%	0.1296±1.8%	3700±0.9%
Air	5.712±1.8%	5162±0.9%	1113±9.3%	1824±9.9%	14.18±1.4%	0.1472±1.3%	6027±0.8%

Table 2. HYPULSE Simulation Parameters

Test Gas	M_1	$Re_{1,d}$	Kn_1	p_2/p_1
CO_2	9.71	33,500	0.00037	18.98
Air	7.93	33,900	0.00028	10.98

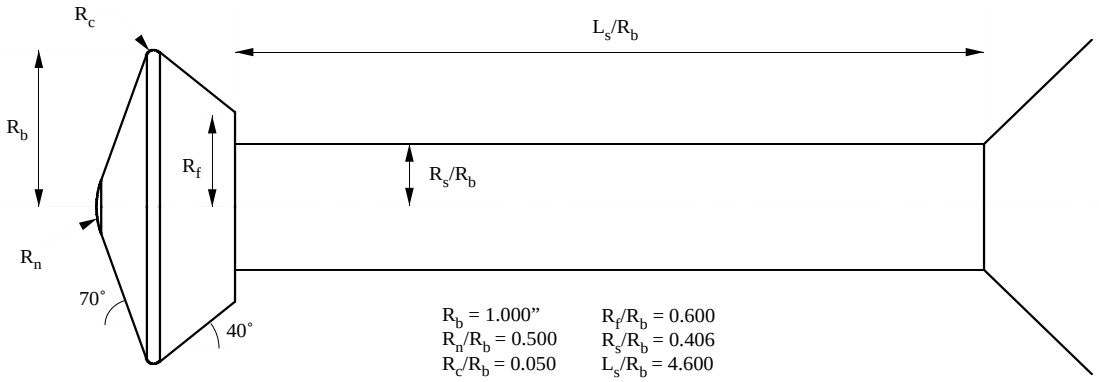

Figure 1. 70-deg Sphere-Cone and Sting Dimensions

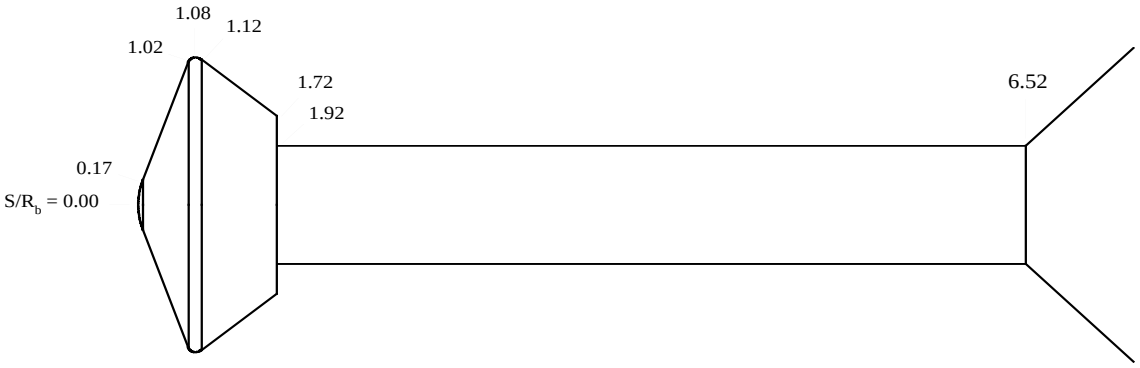

Figure 2. 70-deg Sphere-Cone and Sting Control Points

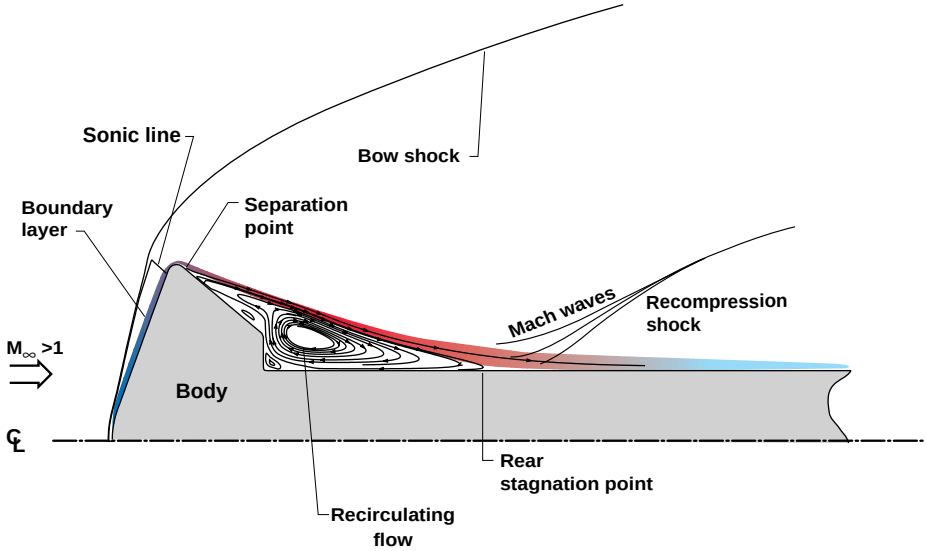

Figure 3. Blunt Body Wake Flow Structure

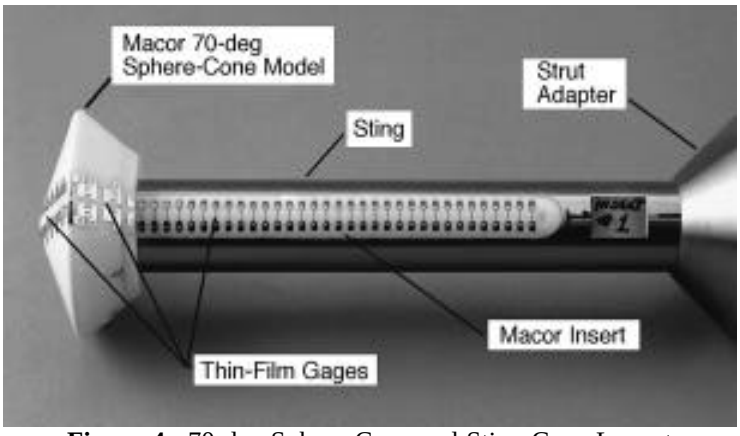

Figure 4. 70-deg Sphere-Cone and Sting Gage Layout

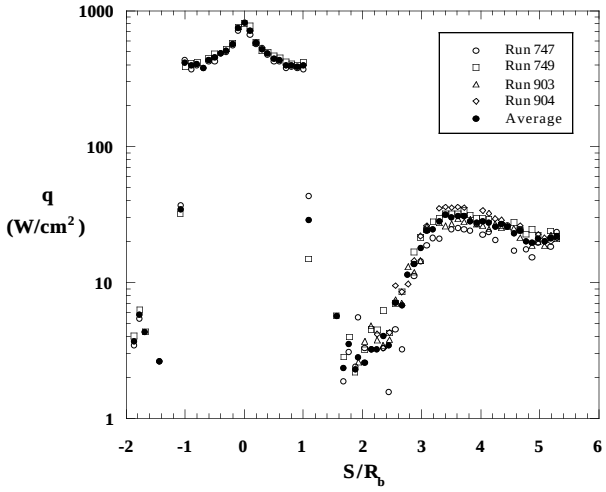

Figure 5. HYPULSE CO_2 Test Data

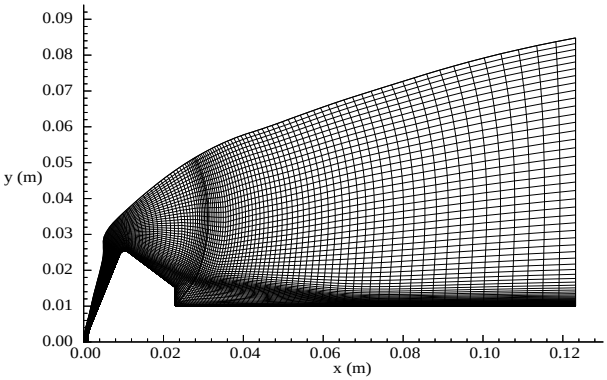

Figure 7a. Shear Layer Adapted 125 x 90 Point Grid for CO_2 Case

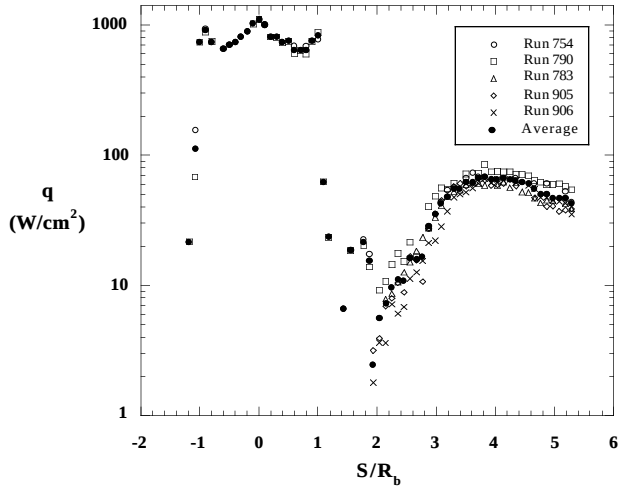

Figure 6. HYPULSE Air Test Data

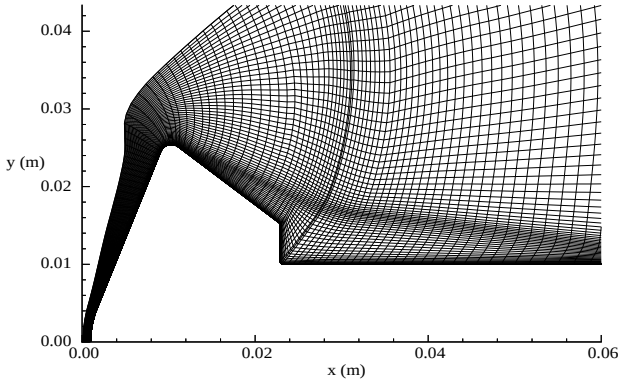

Figure 7b. Shear Layer Adapted 125 x 90 Point Grid for CO_2 Case - Near Wake Details

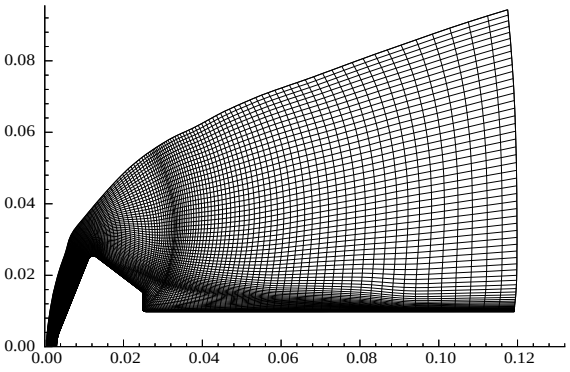

Figure 8a. Shear Layer Adapted 125 x 90 Point Grid for Air Case

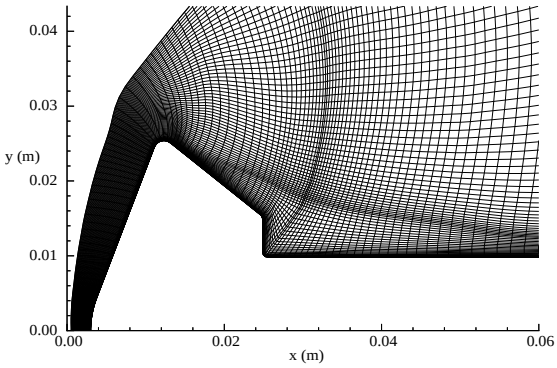

Figure 8b. Shear Layer Adapted 125 x 90 Point Grid for Air Case - Near Wake Details

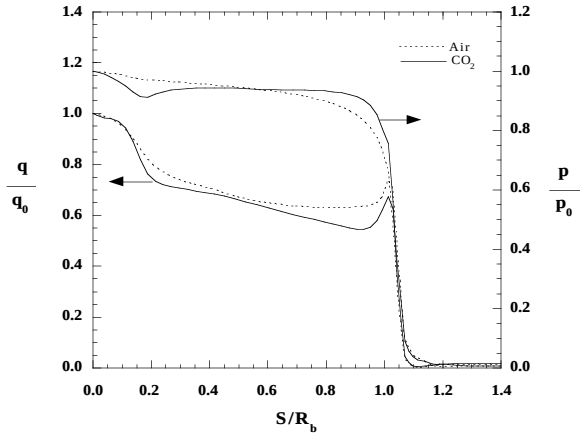

Figure 9a. Normalized Forebody Surface Heating and Pressure Distributions

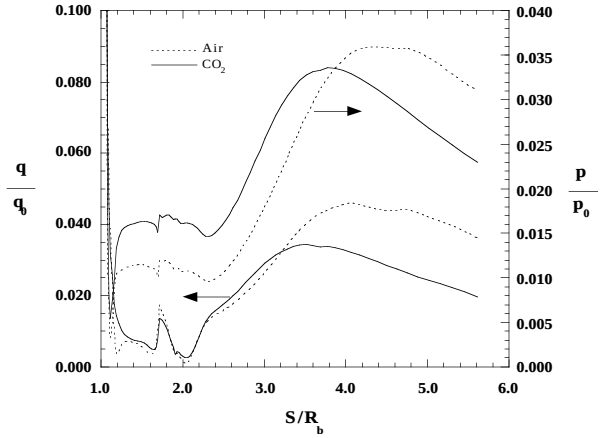

Figure 9b. Normalized Afterbody and Sting Surface Heating and Pressure Distributions

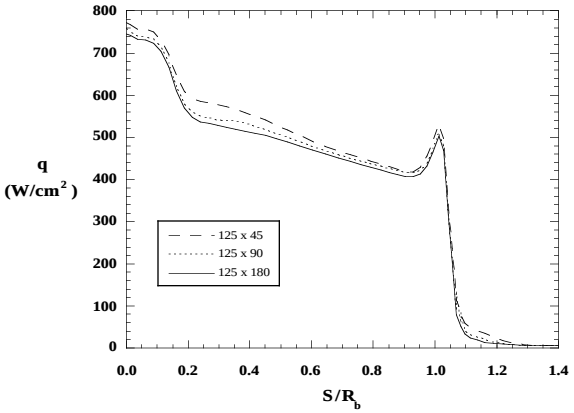

Figure 10a. Effects of Grid Resolution and Adaptation on Forebody Heating for CO_2 Case

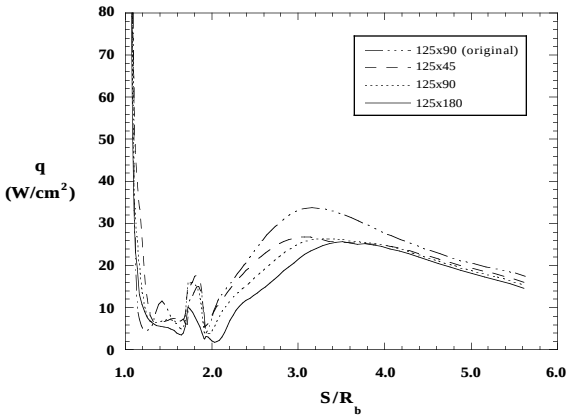

Figure 10b. Effects of Grid Resolution and Adaptation on Wake Heating for CO_2 Case

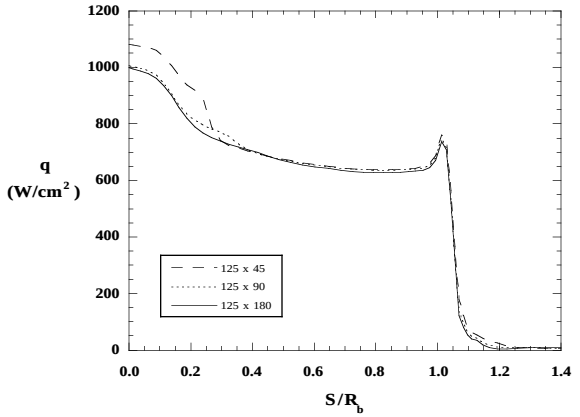

Figure 11a. Effects of Grid Resolution and Adaptation on Forebody Heating for Air Case

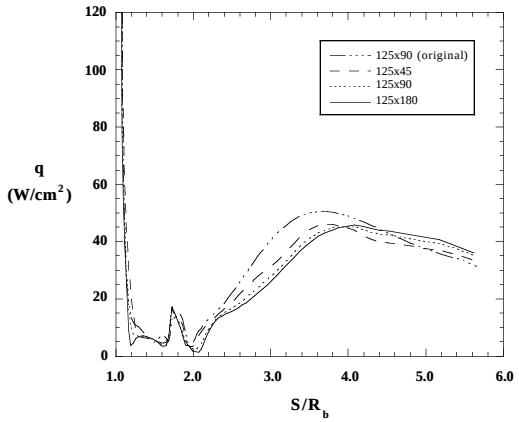

Figure 11b. Effects of Grid Resolution and Adaptation on Wake Heating for Air Case

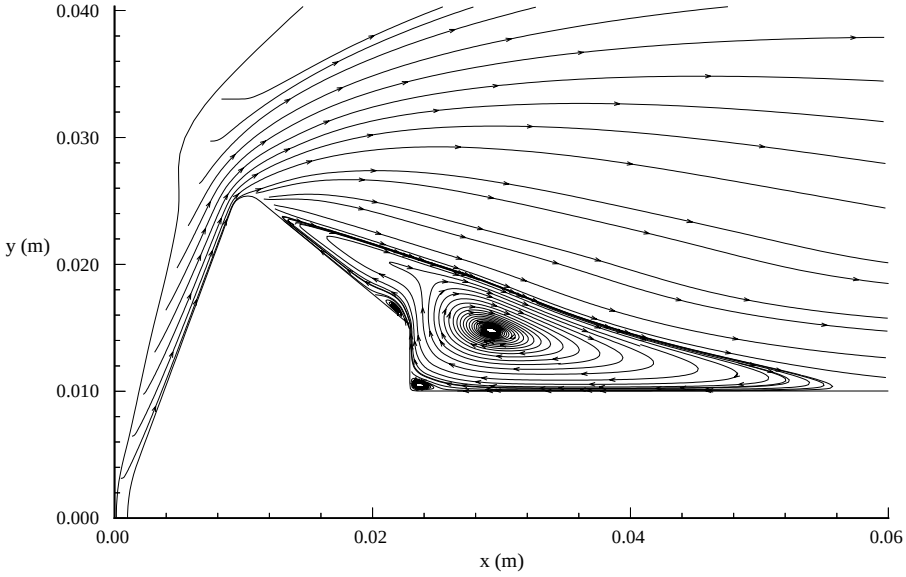

Figure 12. Streamlines in Near Wake Region - CO_2 Case

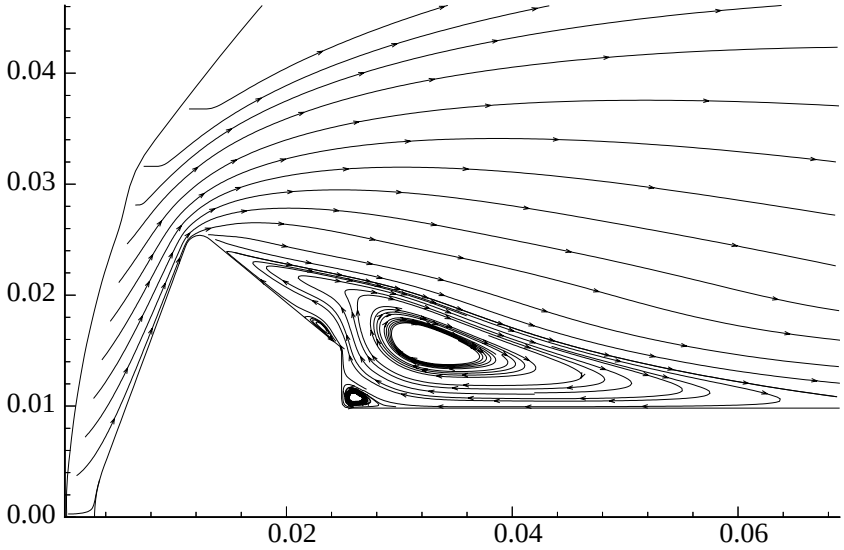

Figure 13. Streamlines in Near Wake Region - Air Case

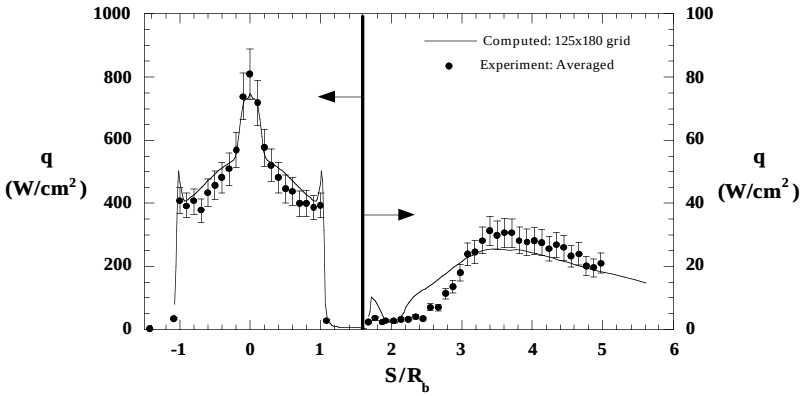

Figure 14. Comparison with Experimental Heating Data - CO_2 Case

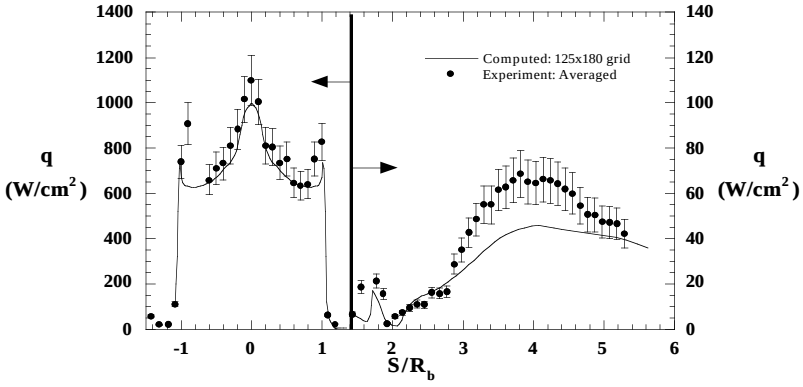

Figure 15. Comparison with Experimental Heating Data - Air Case